

de Haas-van Alphen measurement of the antiferromagnet URhIn₅

Jing Fei Yu,^{1,*} Attila Bartha,² Jeroen Custers,² and Stephen R. Julian^{1,3}

¹*Department of Physics, University of Toronto,
Toronto, Ontario, M5S 1A7, Canada*

²*Department of Condensed Matter Physics, Charles University,
Ke Karlovu 5, 121 16 Praha 2, Czech Republic*

³*Canadian Institute for Advanced Research,
180 Dundas St.W, Toronto, Ontario, M5S 1Z8, Canada*

(Dated: November 10, 2018)

Abstract

We report on the results of a de Haas-van Alphen (dHvA) measurement performed on the recently discovered antiferromagnet URhIn₅ ($T_N = 98$ K), a $5f$ -analogue of the well studied heavy fermion antiferromagnet CeRhIn₅. The Fermi surface is found to consist of four surfaces: a roughly spherical pocket β , with $F_\beta \simeq 0.3$ kT; a pillow-shaped closed surface, α , with $F_\alpha \simeq 1.1$ kT; and two higher frequencies γ_1 with $F_{\gamma_1} \simeq 3.2$ kT and γ_2 with $F_{\gamma_2} \simeq 3.5$ kT that are seen only near the c -axis, and that may arise on cylindrical Fermi surfaces. The measured cyclotron masses range from $1.9 m_e$ to $4.3 m_e$. A simple LDA+SO calculation performed for the paramagnetic ground state shows a very different Fermi surface topology, demonstrating a need for more advanced electronic structure calculations.

I. INTRODUCTION

Uranium based compounds exhibits a wide range of exotic properties, from the unconventional superconductivity in heavy fermion UPt₃¹ to the enigmatic hidden order in URu₂Si₂², and all the way to weakly-correlated metallic behaviour in the uranium metal itself². U atoms possess 5*f* electrons, whose spatial extent is greater than that of the 4*f* valence orbitals of the rare earths, but less than that of 3*d* orbitals of the row four transition metals³. Depending on their environment, the 5*f* electrons can be localized or itinerant (*i.e.* they may or may not be included in the Fermi volume)⁴. Moreover, uranium can have 5*f* valence ranging from 5*f*³ to 5*f*⁰, presenting further opportunities for inter- as well as intra-orbital correlations and complexity.

For some uranium compounds such as the heavy fermion UPt₃¹, the Fermi surface has been mapped and the 5*f* electrons are understood to be itinerant in character. On the other hand, the 5*f* electrons are fully localized in the related compound UPd₃⁵, while quantum oscillation data on the heavy fermion superconductor UPd₂Al₃⁶ has been explained by band structure calculations in which some 5*f* electrons are localized on the U site, while others are itinerant band electrons⁴. Whether and when the 5*f* electrons are localized or itinerant, or partially localized, is still not well understood at present.

The focus of this paper is URhIn₅, a member of the U_{*n*}TX_{3*n*+2} (*n* = 0,1,2; *T* = transition metal; *X* = In, Ga) compounds. They are isostructural with the Ce_{*n*}TX_{3*n*+2} family³. In addition to the open question of the character of the 5*f* electrons, these compounds are also generally interesting because the system has a layered tetragonal structure, which means that adding layers of TX₂ can change the dimensionality from 3D to 2D³.

URhIn₅ has been well characterized along with its bilayer cousin, U₂RhIn₈^{3,7}. It is tetragonal with HoCoGa₅-type structure (P4/mmm). It orders antiferromagnetically at a Néel temperature of $T_N = 98$ K³. The Sommerfeld coefficient is given as $\gamma = 60.7$ mJ mol⁻¹K⁻² with Debye temperature $\Theta_D = 165$ K in Ref. 3, whereas $\gamma = 50$ mJ mol⁻¹K⁻², $\Theta_D = 187$ K are reported by Ref. 8. The Sommerfeld coefficient is similar to that of UNiGa₅⁹, and rather large considering the high Néel temperature. The magnetic moment, $\mu_{\text{eff}} = 3.6\mu_B/U^3$, is close to the U⁴⁺ (5*f*²) moment of $3.58 \mu_B/U^9$. These are again properties very similar to UNiGa₅⁹.

Zero field NMR and NQR measurements have been performed on URhIn₅¹⁰. The nuclear relaxation rate $1/T_1T$ satisfies the Korringa relation just below $T^* \approx 150$ K, which has led

to the suggestion that the $5f$ electrons are localized above T^* and itinerant below¹⁰. The AFM propagation vector is commensurate, with propagation vector $\mathbf{Q} = (1/2, 1/2, 1/2)$ as determined unambiguously by recent neutron diffraction study¹¹. Interestingly, UNiGa₅ also exhibits the same ordering vector¹⁰.

Matsumoto *et al.*⁷ have previously reported dHvA quantum oscillations in URhIn₅. They only observed two frequencies, 1.1 kT and 720 T along [100], with angle dependence suggesting that they both arise on a small ellipsoidal pocket. The presence of small pockets is consistent with the non-magnetic, $5f$ itinerant semi-metal URhGa₅¹², but the authors note that the large specific heat for the antiferromagnetic state of URhIn₅ cannot be explained by this pocket alone, suggesting the likely existence of larger Fermi surfaces undetected by their study. In comparison, quantum oscillation measurements on UNiGa₅ show one cylindrical surface (1.3 kT) along with two larger ellipsoidal surfaces (2.6 kT and 1.6 kT), but additional heavier Fermi surfaces would again be needed to explain the large specific heat⁹. On the other hand, a larger Fermi surface (4 kT) has been detected, in addition to smaller pockets, in UIn₃, the $n = \infty$ member of the $U_n TX_{3n+2}$ family, although additional, multi-connected surfaces are still needed for γ to match experimental values¹³.

Recently, magnetoresistance and Hall resistance also have been measured on URhIn₅¹⁴. The magnetoresistance follows the H^2 behaviour at higher temperatures but deviates from it for temperatures below 30 K¹⁴. At low temperature the magnetoresistance is positive, but the angle dependence, which could reveal the presence of open orbits, has not been reported. The Hall resistance R_H is negative below the Néel temperature (T_N), suggesting that the electron-like carriers dominate electronic transport¹⁴.

Motivated by these previous measurements, we performed a quantum oscillation measurement on high quality URhIn₅ samples. In this paper, we present these results in detail.

II. SAMPLES AND EXPERIMENTAL METHOD

Three high quality crystals of URhIn₅, prepared using the self-flux method³ were used. The samples were X-rayed and characterized using specific heat before the experiment was performed, and they had extremely high RRR (exceeding 200)³, ideal for quantum oscillation measurements.

Modulation field de Haas-van Alphen measurements were carried out on these samples, with field ranges from 9-16 T and at temperatures between 65-2000 mK. The samples were

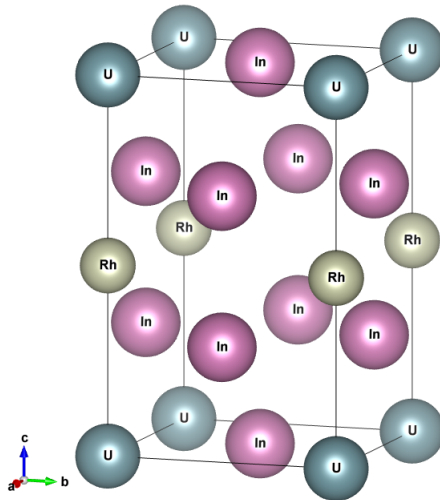


FIG. 1: Crystal structure of URhIn₅, visualized using VESTA software¹⁵

rotated with respect to the applied field in the [001] to [100] plane and the [100] to [110] plane.

III. RESULTS

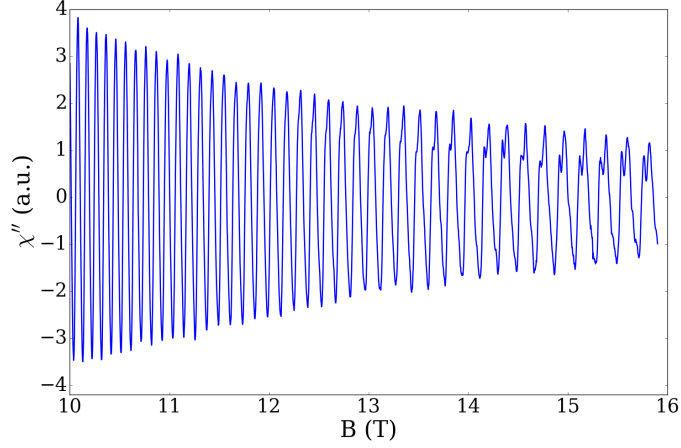
Fig. 2a shows an example of our raw data from 10 to 16 T at 65 mK, with field tilted at 4° from [001], and Fig. 2b shows the Fourier transform of the same set of raw data. A very strong peak at 1.1 kT and its three harmonics can be easily seen. This frequency is labelled α . In addition, expanding the vertical scale in Fig. 2c, other sharp peaks are present as well: at 0.3 kT, 3.2 kT and 3.5 kT. These are labelled β , γ_1 and γ_2 respectively.

The effective mass m^* associated with each extremal orbit can be extracted using the Lifshitz-Kosevich (LK) formula:

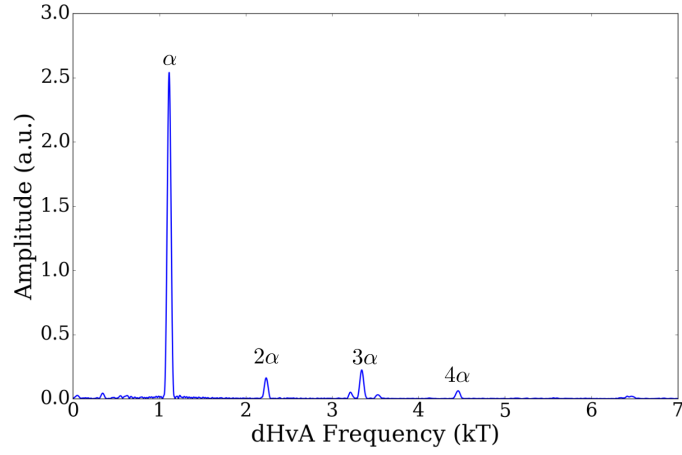
$$A = \frac{Cm^*T/B}{\sinh Cm^*T/B} \quad (1)$$

where $C = \frac{2\pi^2 k_B m_e}{eh}$. Typical fits are shown in Fig. 3. The cyclotron masses found for other directions are summarized in Table I.

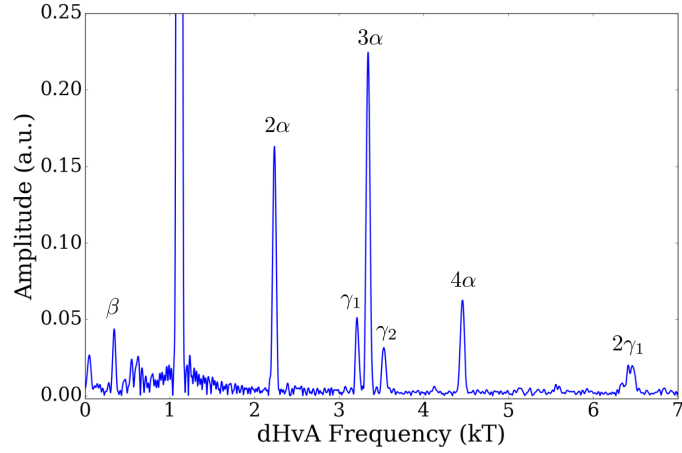
The angle dependence of the dHvA frequencies is shown in Fig. 4. This angle dependence suggests that the β branch, which has very little angle dependence, arises from a nearly spherical Fermi surface. However, the lack of any significant angle dependence may also be a sign of an impurity phase from, say, the inclusion of flux used to grow the sample, or



(a)



(b)



(c)

FIG. 2: **a:**URhIn₅ quantum oscillations from 10 to 16 T, 65 mK. The field is 4° from [001].

b: Fourier transform of the data in (a), showing a dominant α frequency that has been previously reported⁷. **c:** The frequency spectrum of (b) with an expanded vertical scale,

revealing several new frequencies, not observed in previous work.

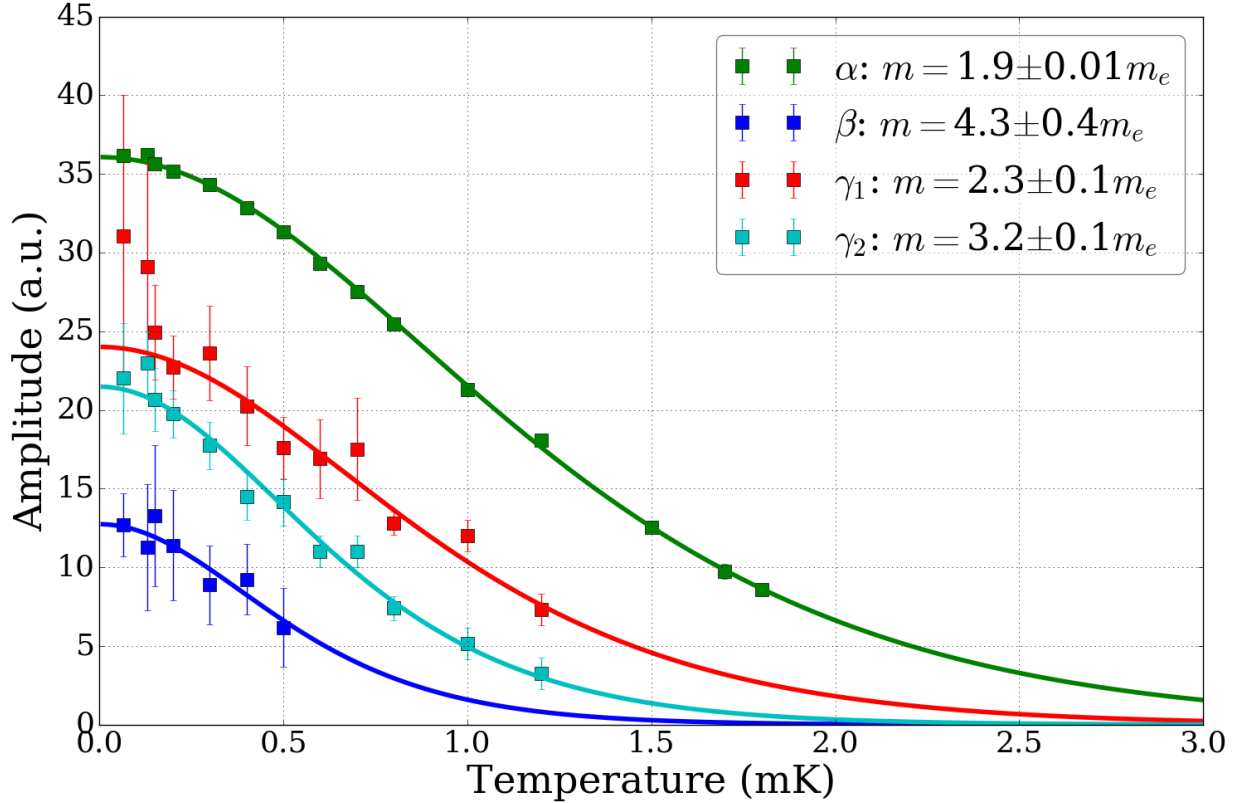


FIG. 3: Mass study of different dHvA frequencies with $B \parallel [001]$, using LK fit. The error bars on the α branch are too small to be seen.

	B \parallel [100]		B \parallel [110]		B \parallel [001]	
Orbit	F (kT)	$m^*(m_e)$	F (kT)	$m^*(m_e)$	F (kT)	$m^*(m_e)$
β					0.3	4.3 ± 0.4
α	1.1	1.5 ± 0.02	1.1	2.0 ± 0.2	1.1	1.9 ± 0.01
γ_1					3.2	2.3 ± 0.1
γ_2					3.5	3.2 ± 0.1

TABLE I: Summary of the experimental dHvA frequencies and fitted cyclotron masses m^* . Missing entries mean that the oscillation were only observed with the applied field along the c -axis.

perhaps a spherical pocket in an impurity phase such U_2RhIn_8 . The α branch splits into two frequencies around 40° . This suggest a distorted sphere that has only one extremal orbit at c -axis, but two extremal orbits beyond a critical angle. The two branches γ_1 and γ_2 are close in frequency and it is natural to think that they arise on the same Fermi surface sheet,

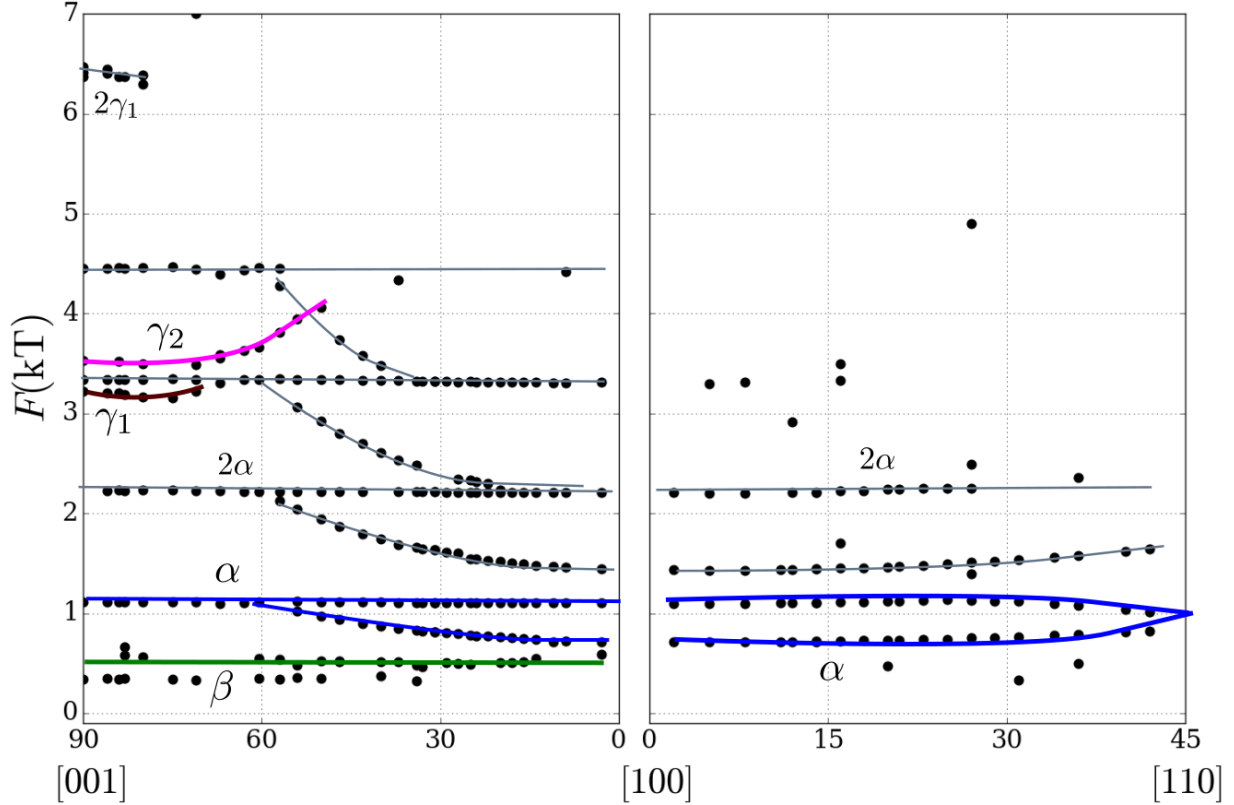


FIG. 4: dHvA frequency F vs θ , where θ is the angle between the magnetic field and the labelled crystalline axes. The data from $[001]$ to $[110]$ plane has been omitted as it is identical to that of $[001]$ to $[100]$.

geometrically this would be certain only if they converge as the angle is rotated away from the c -axis. But the frequency of γ_1 shows only a small upward curvature before it disappears. Thus we cannot rule out the possibility that they are distinct surfaces. γ_1 and γ_2 may arise from cylindrical surfaces, as shown from their upward curvatures. This is supported by the fact that we do not observe these frequencies at $[100]$ or $[110]$, which we would expect if this were a closed surface like α . However, as γ_1 and γ_2 disappear relatively quickly when we rotate away from the c -axis, the evidence is not conclusive.

IV. ANALYSIS AND DISCUSSION

IV.1. Paramagnetic Ground State Calculation

We performed an LDA+SO calculation of URhIn₅'s ground state, using the linearized augmented plane wave (LAPW) scheme that was implemented in the WIEN2k package¹⁶.

	B Direction	F (kT)	$m^*(m_e)$
Band 47	[100]	1.1034	0.73
		1.1516	0.96
	[110]	0.1309	0.83
	[001]	0.2110	0.47
		0.2117	1.02
		0.3034	0.44
		0.5469	0.65
Band 48	[100]	1.0037	1.37
		1.5812	1.42
	[110]	1.1677	1.45
	[001]	1.0745	2.16

TABLE II: dHvA frequencies found using SKEAF, for $B \parallel [100]$, $B \parallel [110]$ and $B \parallel [001]$.

Spin-orbit coupling was turned on, and RK_{\max} was set to 7.0. The resulting Fermi surface is shown in Fig. 5. Using the Supercell K-space Extremal Area Finder (SKEAF)¹⁷ program, dHvA frequencies and approximate effective masses were extracted and are given in Table II. These values do not generally match the experimentally obtained values in Table I, however, band 48 does have a 1.1 kT frequency that is similar to our α branch.

To study this 1.1 kT frequency further, we used SKEAF to find the angle dependence of the frequencies, shown in Fig. 6. Here we can see that the 1.1 kT frequency is a closed ellipsoidal surface similar to our α branch. However, the difference from experiment is that a second, *higher* frequency of 1.5 kT branches out from the main frequency whereas in experimental results, a *lower* frequency branches out. The topology of the two Fermi surfaces are therefore not very similar. While the γ_1 and γ_2 frequencies in our experiment could be coming from cylindrical surfaces, they are almost 10 times larger than the frequencies found by SKEAF in the paramagnetic WIEN2k calculation. It is extremely unlikely that antiferromagnetism could produce larger Fermi surfaces, so our conclusion is that the paramagnetic, all-itinerant Fermi surface is not a good starting point for explaining URhIn₅.

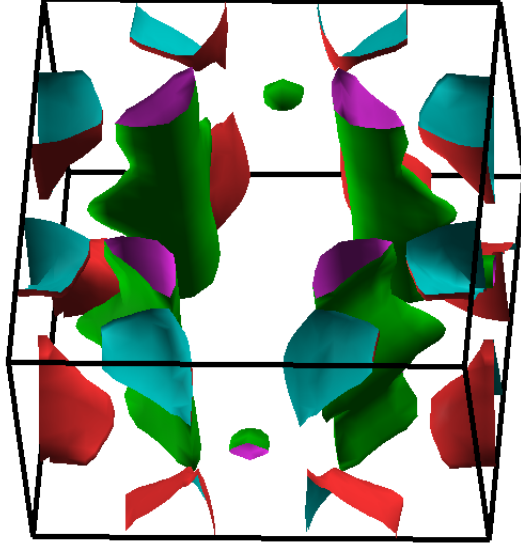


FIG. 5: Fermi surface of the paramagnetic state in a single BZ, calculated by LDA+SO methods using the WIEN2k package¹⁶. Green: band 47; Red: band 48.

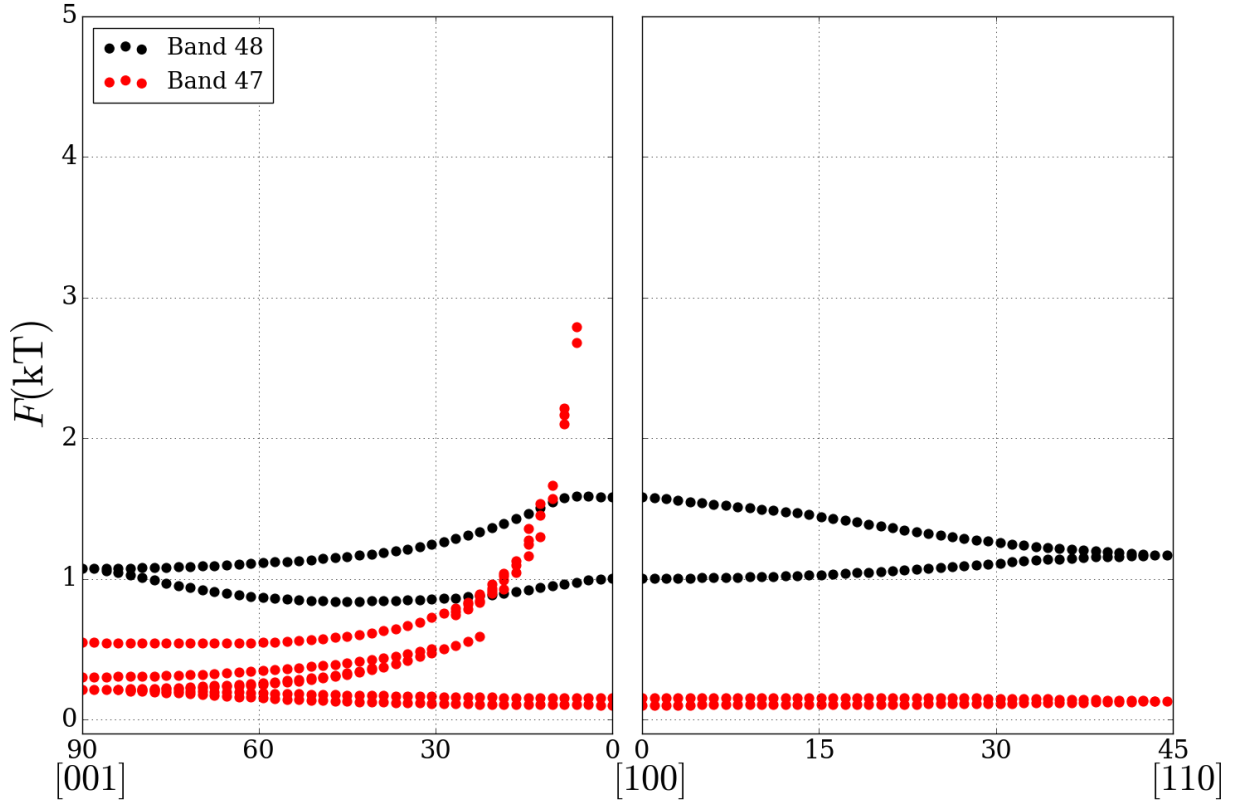


FIG. 6: dHvA frequency F vs θ found by SKEAF for the paramagnetic all-itinerant Fermi surface, where θ is the angle between the magnetic field and the labelled crystalline axes.

For the corresponding surfaces to each band see Fig. 5 and its caption.

IV.2. Fermi Volume Estimation

The total Brillouin zone (BZ) volume is $1.6 \times 10^{30} \text{ m}^{-3}$. If antiferromagnetism doubles the unit cell in the c -axis, the AFM BZ shrinks to $7.8 \times 10^{29} \text{ m}^{-3}$. If we assume all the Fermi surface sheets are spherical so the volume of each sheet is given by $V = 4/3\pi k_F^3$, then given the antiferromagnetic BZ, α occupies 3.2% of the BZ; β occupies 0.4%; γ_1 occupies 16% and γ_2 occupies 19% of the Brillouin zone. If we assume γ_1 and γ_2 are cylindrical surfaces and their volumes are given by $S_F \times 2\pi/(2c)$ where S_F is the area enclosed by the cylinder and given by the dHvA frequency, c is the c -axis lattice parameter, and $2\pi/(2c)$ is the height of the AFM BZ, the volumes of γ_1 and γ_2 become 17% and 18% of the total BZ volume, respectively. In total these Fermi surface sheets occupy nearly 40% of the total AFM BZ, if we assume there is only one copy of each Fermi surface in the BZ. As noted in the next section, however, it is probable that there are multiple copies of at least some Fermi surfaces.

IV.3. Sommerfeld Coefficient Estimation

We can estimate the Sommerfeld coefficient $C/T = \gamma$ from the Fermi surfaces obtained. If we make the simplifying assumption that the frequencies at [001] correspond to spherical Fermi surfaces, so that the extremal area is given by $S_F = \pi k_F^2$, then α would contribute $1.7 \text{ mJ mol}^{-1}\text{K}^{-2}$; β would contribute $2.1 \text{ mJ mol}^{-1}\text{K}^{-2}$; γ_1 would contribute $3.6 \text{ mJ mol}^{-1}\text{K}^{-2}$ and γ_2 would contribute $5.2 \text{ mJ mol}^{-1}\text{K}^{-2}$. This sums up to $12.6 \text{ mJ mol}^{-1}\text{K}^{-2}$ if we assume one sheet each, whereas the experimental value is around $50\text{-}60 \text{ mJ mol}^{-1}\text{K}^{-23,8}$.

If, however, we assume that γ_1 and γ_2 are distinct, cylindrical, Fermi surfaces. Then their specific heat contributions are no longer k_F dependent and they rise to $7.6 \text{ mJ mol}^{-1}\text{K}^{-2}$ for γ_1 and $10.6 \text{ mJ mol}^{-1}\text{K}^{-2}$ for γ_2 . The total C/T contribution then rises to $22 \text{ mJ mol}^{-1}\text{K}^{-2}$ if we assume one copy of each sheet. This is still much too small. Thus we assume multiple copies of each sheet. For example, $4 \times \alpha$, $4 \times \beta$, $2 \times \gamma_1$ and $2 \times \gamma_2$ gives $52 \text{ mJ mol}^{-1}\text{K}^{-2}$, in the range of the observed Sommerfeld coefficient, and the total BZ occupation will be around 84%. If, as seems more likely, γ_1 and γ_2 are extremal orbits on the same cylindrical Fermi surface, then we can have $4 \times \gamma$ instead of $2 \times \gamma_1$ and $2 \times \gamma_2$ with an average contribution of $9.1 \text{ mJ mol}^{-1}\text{K}^{-2}$ per sheet gives the same result. This scenario would account for all of the specific heat, but the BZ would be very packed. The only other possibility is that there are heavy orbits (*i.e.* hot spots) on the Fermi surface sheets that we have observed, or else

other heavy surfaces that we have not observed. A better estimate of γ will be obtained once we have reliable band-structure calculations.

IV.4. Comparisons to Previous Studies and Other Related Compounds

Comparing our results to the earlier dHvA study on URhIn₅ by Matsumoto *et al.*⁷, the frequency α and its splitting at higher angles were seen in both experiments. The angle dependence, which is indicative of an ellipsoidal Fermi surface, agrees well. In our experiment however, we also observed two larger Fermi surface sheets, γ_1 and γ_2 , as well as one additional small spherical pocket β . While the total contribution from the observed sheets to specific heat remains well under the experimental value of $\gamma = 50 - 60 \text{ mJ mol}^{-1}\text{K}^{-2}$, we can at least consider the possibility of some combination of these sheets as mentioned in the section above, that will make up the missing specific heat contribution. The observation of these larger sheets also suggests that URhIn₅ is very different from the non-magnetic, $5f$ -itinerant semi-metal URhGa₅ which has only small pockets and small specific heat^{7,12}.

In Ref. 7, a comparison was made to a reference compound ThRhIn₅, which has the same crystal structure but does not have $5f$ electrons. ThRhIn₅ has very large Fermi surfaces (up to 7 kT) and with strong angle dependence that would be expected for quasi-cylindrical surfaces^{7,18}. These are considerably larger than our observations. However, as γ_1 and γ_2 are suggestive of being cylindrical surfaces, it may be that the electronic structure of URhIn₅ is not as drastically different from ThRhIn₅ as previously thought⁷.

UNiGa₅ is another antiferromagnet in this family, with a Néel temperature $T_N = 85.5 \text{ K}$ and a Sommerfeld coefficient $\gamma = 30 \text{ mJ mol}^{-1}\text{K}^{-29}$. Its Fermi surface has also been mapped using dHvA. In URhIn₅, our α surface has a very different angular dependence from that of any of the ellipsoidal Fermi surfaces in UNiGa₅. The largest cylindrical Fermi surface in UNiGa₅, on the other hand, also has much smaller cross-section for field along the c -axis than our γ_1 and γ_2 surfaces. Whereas Tokiwa *et al.* see clear evidences of cylindrical Fermi surfaces⁹, we were unable to follow our γ_1 and γ_2 frequencies far enough to confirm the $1/\cos\theta$ dependence expected for a cylindrical Fermi surface, but on balance it seems very likely that they arise on a cylindrical surface. The effective masses of UNiGa₅ at around 1.4 to 3.1 m_e are, however, similar to those found for URhIn₅⁹ There are no calculations available for the antiferromagnetic ground state of UNiGa₅, and the paramagnetic state calculation does not match the experimental results⁹.

As mentioned in the introduction, another related compound to URhIn₅ is UIn₃. This compound is also an antiferromagnet and orders at $T_N = 88$ K¹³. It has a Sommerfeld coefficient of $\gamma = 40$ mJ mol⁻¹K⁻². The Fermi surface has been mapped, and no cylindrical Fermi surfaces were found¹³. The angle dependence does not resemble our findings for URhIn₅, and the effective masses of UIn₃ range from 9.8 to 33 m_e , which are significantly larger than those of URhIn₅. However, as is the case of UNiGa₅, the lack of reliable band structure calculations for URhIn₅ and UIn₃¹³ makes these comparisons quite speculative.

V. CONCLUSION

We remark that there are major discrepancies between the calculated $5f$ all-itinerant Fermi surface and the experimentally obtained dHvA frequencies, and the cyclotron masses also differ. The present results cannot be fully explained by the paramagnetic calculation and it is therefore highly desirable that a detailed band structure calculation be carried out for the antiferromagnetic ground state.

VI. ACKNOWLEDGEMENTS

J. C. would like to acknowledge many helpful discussions with M. Diviš. This work was generously supported by NSERC and CIFAR of Canada, Canada Research chair, the Czech Science Foundation Grant No. P203/12/1201 and the Charles University project CA UK Grant No. 128317.

* email: jfeiyu@physics.utoronto.ca

¹ G. J. McMullan, P. M. C. Rourke, M. R. Norman, A. D. Huxley, N. Doiron-Leyraud, J. Flouquet, G. G. Lonzarich, A. McCollam, and S. R. Julian, *New Journal of Physics* **10**, 053029 (2008), arXiv:0803.1155v2.

² J. Mydosh and P. Oppeneer, *Philosophical Magazine* **94**, 3642 (2014), arXiv:1405.1625.

³ A. Bartha, M. Kratochvílová, M. Dušek, M. Diviš, J. Custers, and V. Sechovský, *Journal of Magnetism and Magnetic Materials* **381**, 310 (2015), arXiv:1501.02154.

⁴ G. Zwirnagl, A. Yaresko, and P. Fulde, *Physical Review B* **68**, 052508 (2003).

- ⁵ Y. Tokiwa, K. Sugiyama, T. Takeuchi, M. Nakashima, R. Settai, Y. Inada, Y. Haga, E. Yamamoto, K. Kindo, H. Harima, and Y. Onuki, *Journal of the Physical Society of Japan* **70**, 1731 (2001).
- ⁶ Y. Inada, H. Yamagami, Y. Haga, K. Sakurai, Y. Tokiwa, T. Honma, E. Yamamoto, Y. nuki, and T. Yanagisawa, *Journal of the Physical Society of Japan* **68**, 3643 (1999).
- ⁷ Y. Matsumoto, Y. Haga, N. Tateiwa, E. Yamamoto, N. Kimura, H. Aoki, and Z. Fisk, in *Proceedings of the International Conference on Strongly Correlated Electron Systems (SCES2013)*, Vol. 3 (*Journal of the Physical Society of Japan*, 2014) p. 011097.
- ⁸ Y. Matsumoto, Y. Haga, N. Tateiwa, H. Sakai, T. D. Matsuda, E. Yamamoto, and Z. Fisk, *Physical Review B* **88**, 045120 (2013).
- ⁹ Y. Tokiwa, Y. Haga, E. Yamamoto, D. Aoki, N. Watanabe, R. Settai, T. Inoue, K. Kindo, H. Harima, and Y. Onuki, *Journal of the Physical Society of Japan* **70**, 1744 (2001).
- ¹⁰ H. Sakai, S. Kambe, Y. Tokunaga, Y. Matsumoto, N. Tateiwa, Y. Haga, and Z. Fisk, *Physical Review B* **88**, 045123 (2013).
- ¹¹ A. Bartha, M. Klicpera, P. Čermák, B. Oluaddiaf, P. Javorský, and J. Custers, manuscript in preparation.
- ¹² S. Ikeda, Y. Tokiwa, T. Okubo, Y. Haga, E. Yamamoto, Y. Inada, R. Settai, and Y. Onuki, *Journal of Nuclear Science and Technology* **39**, 206 (2002).
- ¹³ Y. Tokiwa, D. Aoki, Y. Haga, and E. Yamamoto, *Journal of the Physical Society of Japan* **70**, 3326 (2001).
- ¹⁴ Y. Haga, Y. Matsumoto, J. Pospíšil, N. Tateiwa, E. Yamamoto, T. Yamamura, and Z. Fisk, *Journal of Physics: Conference Series* **807**, 012015 (2017).
- ¹⁵ K. Momma and F. Izumi, *Journal of Applied Crystallography* **44**, 1272 (2011).
- ¹⁶ P. Blaha, K. Schwarz, G. Madsen, D. Kvasnicka, and J. Luitz, *WIEN2k, An Augmented Plane Wave+Local Orbitals Program for Calculating Crystal Properties* (Karlheinz Schwartz, Universitat Wien, Austria, 2011).
- ¹⁷ P. Rourke and S. Julian, *Computer Physics Communications* **183**, 324 (2012).
- ¹⁸ T. D. Matsuda, Y. Haga, E. Yamamoto, S. Ikeda, H. Shishido, R. Settai, H. Harima, and Y. Onuki, *Journal of the Physical Society of Japan* **76**, 064712 (2007).